

# Robots Autonomously Detecting People: A Multimodal Deep Contrastive Learning Method Robust to Intraclass Variations

Angus Fung, Beno Benhabib, and Goldie Nejat, *Member, IEEE*

**Abstract**—Robotic detection of people in crowded and/or cluttered human-centered environments including hospitals, long-term care, stores and airports is challenging as people can become occluded by other people or objects, and deform due to variations in clothing or pose. There can also be loss of discriminative visual features due to poor lighting. In this paper, we present a novel multimodal person detection architecture to address the mobile robot problem of person detection under intraclass variations. We present a two-stage training approach using 1) a unique pretraining method we define as Temporal Invariant Multimodal Contrastive Learning (TimCLR), and 2) a Multimodal Faster R-CNN (MFRCNN) detector. TimCLR learns person representations that are invariant under intraclass variations through unsupervised learning. Our approach is unique in that it generates image pairs from natural variations within multimodal image sequences, in addition to synthetic data augmentation, and contrasts crossmodal features to transfer invariances between different modalities. These pretrained features are used by the MFRCNN detector for finetuning and person detection from RGB-D images. Extensive experiments validate the performance of our DL architecture in both human-centered crowded and cluttered environments. Results show that our method outperforms existing unimodal and multimodal person detection approaches in terms of detection accuracy in detecting people with body occlusions and pose deformations in different lighting conditions.

**Index Terms**— Robotic Person Detection, RGB-D Features, Deep Contrastive Learning, Intraclass Variations, Cluttered/Crowded Environments

## I. INTRODUCTION

Robots need to be able to autonomously detect multiple people in various human-centered environments in order to engage in effective human-robot interactions. Namely, person detection applications range from long-term care, retirement and private home settings, where interactive robots search for users to provide reminders and assistance with activities of daily living [1]–[3], product searches in big-box retail stores [4], [5], and direction guidance in airports [6] and hospitals [7], [8]. Furthermore, in disaster scenes, rescue robots can search to find trapped victims under rubble [9].

In general, human-centered environments can be crowded and cluttered with multiple dynamic people and objects, resulting in person and body part occlusions [9]. Furthermore, as people move or interact in the environment, they can undergo deformation due to both variations in clothing and

body articulation [10]. These environments can also have variable illumination due to both natural and artificial lighting sources [11], which can result in appearance changes despite intrinsic properties of the person (*e.g.*, shape) not changing [11]. These variations can be defined as intraclass variations.

Classical machine learning approaches have been used by robots to address the person detection problem [12]–[15]. The majority of these approaches use a two-stage method to first extract a set of expert handcrafted features, such as HOG features [12]–[15], from upright people [16], and then train a supervised learning model to classify people in both indoor and outdoor environments. However, HOG features can only be used in applications where people maintain a fixed orientation to the robot [16]. Yet, people exhibit a variety of poses throughout the day, including sitting, lying down, etc.

Deep learning (DL) approaches address the limitations of classical learning methods by autonomously learning feature extraction, without having human experts extract handcrafted features. Thus, they can generalize to people in different poses and postures within varying environments [17]. DL methods use convolutional neural networks (CNN) to learn person feature representations in a hierarchical structure [18], [19].

To-date, robots use existing DL-based detection methods built on off-the-shelf *object detectors* to detect people in both indoor/outdoor environments. Object detection methods used include: 1) You Only Look Once (YOLO) [20], 2) Single Shot MultiBox Detector (SSD) [21], 3) RetinaNet [9], and 4) Faster R-CNN (FRCNN) [22]. These DL methods use RGB images from a single onboard camera on a robot for feature extraction by a *unimodal* CNN to detect people; however, these methods have difficulty in cluttered environments with varying illumination, as visual features necessary for discriminating people from their backgrounds become less prominent. Furthermore, these DL methods use *off-the-shelf pretrained RGB weights* to initialize the CNN models. This limits their application to unimodal CNNs as off-the-shelf multimodal pretrained weights currently do not exist [23], [24].

To address intraclass variations in DL-based person detection methods, data augmentation has been used to increase the amount of training data [9]. However, data augmentation cannot capture the majority of variations due to low probability of occurrence [25]. Unsupervised contrastive learning (CL), on the other hand, can be used to address people and environment variations by directly pretraining a multimodal DL model to learn invariant features from scratch and from unlabeled data [26]. CL approaches have been used to learn feature representation invariances by contrasting between images of different viewpoints of the same static objects in constant lighting conditions [27]. Thus, they have the potential to learn representations which are invariant to intraclass variations if image pairs of the same scene under

This research is supported by the Natural Sciences and Engineering Research Council of Canada (NSERC), AGE-WELL Inc., and the Canada Research Chairs (CRC) program. Authors are with the Autonomous Systems and Biomechatronics Lab in the Department of Mechanical and Industrial Engineering at the University of Toronto, 5 King's College Road, Toronto, ON, M5S 3G8 Canada. (Email: angus.fung@mail.utoronto.ca, {benhabib, nejat}@mie.utoronto.ca).

different conditions can be generated. Unlabelled data is relatively inexpensive to collect as a robot can be deployed to autonomously collect such multimodal data directly from human-centered environments without the need for manual labelling. Recently, CL methods have been used in a handful of robotic applications [27], [28], [32]. However, to-date, CL has not been applied to the robotic person detection problem.

In this paper, we present a novel multimodal DL person detection architecture for mobile robots which uses a two-stage training approach consisting of: 1) contrastive learning for pretraining, and 2) Multimodal Faster R-CNN (*MFRCNN*) for finetuning. For prediction, the trained *MFRCNN* is used for autonomous people detection from RGB-D data. We have developed a new pretraining method, Temporal Invariant Multimodal Contrastive Learning (*TimCLR*), to pretrain a multimodal CNN model from unlabelled RGB-D data in human-centered environments. *TimCLR* incorporates intraclass variations by generating multimodal image pairs from sampling video frames within a short temporal interval, and contrasting person representations within and between modalities, in addition to augmented data. This captures the natural variations in appearance (lighting, occlusions and pose deformations) as people move in their environments. Our overall approach is unique in that it uses contrastive learning to combine natural variations in the environment obtained from multimodal features, as well as incorporates a fusion backbone to contrast multimodal features. Thus, our approach does not require pretrained RGB weights or expert handcrafted mappings. We present extensive experiments to verify that our DL architecture outperforms existing DL detection methods in both human-centered crowded (with dynamic people) and cluttered (with objects) environments.

## II. RELATED WORKS

In this section, we discuss the existing DL methods developed for robots to autonomously detect multiple dynamic people in human-centered environments. We further introduce CL methods and their current robotic applications.

### A. Person Detection by Robots

Existing person detection methods for robotic applications consist of: 1) single-stage detectors including YOLO [9], [20], [29], [30], SSD [9], [21], and RetinaNet [9]; and 2) two-stage detectors including Faster R-CNN [7]–[9].

In single-stage detectors, every position in an image is considered as region proposals for containing potential people [9]. A backbone CNN with additional layers is used to predict the bounding box of a person [9]. For example, in [20], [29], and [30], YOLO detectors used RGB images to detect a person in indoor environments for a robot to follow the person to provide assistance. In [21], an SSD detector detected multiple people in RGB images for person following by a mobile robot in indoor environments. All detectors were initialized using off-the-shelf RGB weights which were pretrained on ImageNet with images of general objects [19].

In two-stage detectors, a first stage region proposal network (RPN) is used to generate region proposals, followed by a second stage, where these proposals are classified and regressed [9]. For example, in both [7] and [8], a FRCNN

detector was used to find people with different mobility aids in populated environments (e.g., hospitals, airports). People were detected in either RGB or depth images using RGB and depth networks which were pretrained on ImageNet. As off-the-shelf pretrained RGB weights require 3 input channels, the depth images were preprocessed using ColorJet. This colorized the depth images by distributing depth data based on distance. Both networks were trained on the Mobility Aids dataset [7] consisting of expert annotated RGB-D images of people with different aids in a hospital obtained from a mobile robot.

In our own previous work [9], several single and two-stage deep networks were compared for person body part detection in cluttered urban search and rescue (USAR) settings. The detectors were used to identify six body parts (arm, foot, hand, head, leg, torso) from RGB and depth images. All networks were trained on RGB, depth, and RGB-D data, using off-the-shelf RGB weights pretrained on ImageNet. The RGB-D data was trained with data-level fusion where RGB and depth were fused through compression at the input into 3 channels that consist of the grayscale of the RGB image, and the upper and lower 8 bits of the 16-bit depth image. The networks were trained on a small dataset consisting of RGB-D images, collected by a mobile robot in an indoor USAR-like environment consisting of fully visible and partially occluded body parts of both mannequins and humans. The architecture was tested in a different USAR-like environment.

### B. Contrastive Learning Methods

Contrastive learning (CL) is a DL method which learns feature representations through similarities or dissimilarities between pairs of images without the need for expert labels by maximizing the agreement between two views of the same scene [31]. It is commonly used to pretrain general representations which can be transferred through finetuning to downstream tasks such as object detection [26] or robot manipulations [27]. CL methods can be categorized based on their input type: 1) image-based [26], [28], [31], or 2) video-based [27], [32]. Image-based methods generate different views by applying random data augmentation to the same image [33]. Video-based methods generate different views based on natural transformations from frames within a video sequence [27] or from different video sequences [32]. These views are optimized by the contrastive loss, which maximizes the agreement between two views of the same sample and the disagreement between views of other samples (negative pairs) [33].

CL methods have been incorporated in a handful of robotic applications [27], [28], [32]. In [27], a video-based CL method was used to learn robot manipulation behaviors of pouring liquids by imitating human interactions from videos collected from two smartphones. A network was pretrained to learn viewpoint-invariant features from RGB images by maximizing representations between different viewpoints of the same scene from different video sequences taken at the same time. Reinforcement learning (RL) was used to learn policies from the pretrained network. Experiments were conducted in an indoor room with constant lighting.

In [32], a video-based CL method was used to directly train a network for object discovery by a mobile robot to learn

representations of unseen toys and kitchen appliances. This included recognizing and matching an instance of an unknown object seen previously to learn viewpoint-invariant features (e.g., texture, shape) without any human labels. The method extracted features from a pair of random RGB images in a video sequence captured from an HD camera on a mobile robot, and then maximized the representation between each object and its closest neighbor. Experiments were conducted in different rooms in a house and office environment with constant lighting to match static objects to reference objects.

In [28], an image-based CL method was used to directly train a RL architecture for autonomous robot navigation in a smoked filled environment. CL was applied to learn smoke-invariant representations from LIDAR and radar data, where the latter was robust to smoke. Positive pairs were generated by taking one view from radar, and the other view from LIDAR. CL was optimized jointly with the RL policy. Experiments were conducted in a cardboard maze.

The image-based method MoCo v3 [26] has been applied to the general problem of object detection, using synthetic data augmentation to learn general object representations during pretraining on ImageNet. These features are transferred to a detection task, for example, on the COCO dataset [34] with 80 object classes. In particular, MoCo v3 learns representations using an encoder and momentum encoder [26]. MoCo v3 generates image pairs by applying two sets of random data augmentations on the same RGB image [26]. Each image is passed into one of the encoders to generate a pair of representations. The contrastive loss is then used to maximize the similarity between those representations [26]. Results have shown that MoCo v3 outperforms the other image-based unsupervised methods, and even supervised pretraining methods in terms of detection accuracy [26], [31]. Thus, MoCo v3 has the potential to be applied to the robotic problem of person detection. However, it only considers artificial data augmentation to generate different views and does not incorporate temporal variations.

### C. Summary of Limitations

Existing robotic person detection methods have used unimodal CNNs with off-the-shelf pretrained RGB weights trained on ImageNet, with the exception of [9]. As these unimodal CNN approaches only incorporate RGB information, they can have difficulty detecting people under poor illumination as discriminative person features in images can become less noticeable due to underexposure [35]. The depth-only CNN approach [8] is robust to illumination, however, can only capture person features that have unique distance information from surrounding objects and people.

While the approach in [9] incorporates multimodal RGB-D data, it uses pretrained RGB weights and handcrafted heuristics to compress the RGB-D data from 4 channels to 3. To avoid information loss due to compression, off-the-shelf multimodal pretrained weights are required; however, they do not exist currently. Although an alternative approach can be to train from scratch using supervised DL methods, existing multimodal robotic datasets with hand-labelled detection annotations are small, ranging from 572 to 17,000 images [8], [9], [36]. These are significantly smaller than the ImageNet

dataset with 1 million images, which can result in significant overfitting during training [37]. Instead of using off-the-shelf weights, handcrafted heuristics, or large amounts of annotated data, CL can be used, as a first stage, to pretrain multimodal models from unlabeled data.

Image-based CL methods do not consider intraclass variations. Video-based CL methods, used in a handful of robotic applications, consider temporal variations within RGB images, but have mainly been applied to constant lighting environments with static objects [27], [32]. Moreover, using only temporal variations, without data augmentation, may degrade the quality of learned representations due to feature suppression [38], as cues such as color distributions are similar between frames in a video. Thus, the network may learn to use these cues to contrast different views instead of learning feature invariances.

To address the above limitations, we present a modified MoCo v3 CL method to generate image pairs by uniquely combining both synthetic data augmentations and temporal variations from multimodal image frames within a short temporal interval. In addition to contrasting features between modalities to transfer invariances learned from one modality to the other, we use a fusion backbone to contrast multimodal features. We incorporate the above as our novel first stage *TimCLR* pretraining method, whose weights are then transferred to the second stage *MFRCNN* detector for finetuning and detecting people from RGB-D images.

## III. PERSON DETECTION METHODOLOGY

We propose a person detection architecture to detect multiple dynamic people or body parts from RGB and depth images in human-centered environments. The proposed architecture, Fig. 1, consists of two training stages: 1) a *TimCLR* stage, using CL for unsupervised pretraining to learn RGB-D person and body part representations which are robust to intraclass variations, and 2) a *MFRCNN* stage for supervised finetuning using the pretrained *TimCLR* model. For prediction, RGB-D images are passed into the trained *MFRCNN* detector to detect multiple people or body parts in the environment.

The *TimCLR* stage uses an unlabeled sequence of RGB-D images as inputs. RGB-D image pairs are generated by the *Sampling* module by randomly sampling frames within a short temporal interval. These pairs capture natural variations in the environment by considering similar scenes under different conditions. In addition to considering natural variations, the *Augmentation* module applies synthetic data augmentation to each RGB-D image in the image pair. The *Multimodal Feature Extraction & Fusion (MFEF)* module passes RGB-D images into different encoders to extract RGB, depth, and RGB-D person feature representations. The *Crossmodal* module maximizes the contrastive loss of RGB-D representations generated by a fusion backbone, as well as between RGB and depth representations generated by unimodal backbones. The weights of the network obtained through backpropagation are transferred to the next stage.

The *MFRCNN* stage uses labelled RGB-D images and the pretrained weights from *TimCLR* as inputs for finetuning. It adopts the FRCNN structure of a region proposal and refinement stage. Specifically, we replace the RGB backbone

used in FRCNN with a subset of the backbone layers used in *TimCLR*. We also replace the layers used in the refinement stage with the fusion backbone from *TimCLR*. The weights from *TimCLR* are used to initialize *MFRCNN* for training. The *MFEF* module extracts and fuses RGB and depth person features to detect multiple people (or body parts) as they move in a human-centered environment. *MFRCNN* outputs a bounding box for each detected person within the image.

#### A. Temporal Invariant Multimodal Contrastive Learning

*TimCLR* extends MoCo v3, to provide different views by combining both synthetic data augmentation and natural variations in the environment obtained from a sequence of RGB and depth images. By combining these, we minimize the quality degradation of learned representations due to feature suppression [38]. The 4 main modules of the *TimCLR* stage are discussed in detail below.

##### 1) Sampling

The *Sampling* module samples pairs of RGB and depth images from a multimodal dataset  $\mathcal{D}$ , consisting of sequences of unlabeled images containing people performing activities in a human-centered environment. These sequences capture people (and body parts) undergoing natural variations in occlusion, pose deformation, and lighting. Image pairs are sampled within a short temporal interval  $\Delta_t$ . In practice, these pairs are sampled either from short video sequences of length  $\Delta_t$  or from short segments of length  $\Delta_t$  from longer duration full videos. Let  $(\mathbf{x}_1^{RGB}, \mathbf{x}_1^D)$  be an RGB-D image sampled at time  $t_1$ , and  $(\mathbf{x}_2^{RGB}, \mathbf{x}_2^D)$  at time  $t_2$ , then a pair of RGB-D images is represented as:

$$((\mathbf{x}_1^{RGB}, \mathbf{x}_1^D), (\mathbf{x}_2^{RGB}, \mathbf{x}_2^D)) \sim \mathcal{D} \times \mathcal{D}. \quad (1)$$

##### 2) Augmentation

The *Augmentation* module applies a set of transformations to each sample pair of images from Eq. (1), which relate two multimodal views representing the same people under different conditions. Namely, the following MoCo v3 transformations are randomly applied [26]: cropping, color jittering, grayscaling, gaussian blurring, and horizontal flipping. Let  $\mathbf{T}_1, \mathbf{T}_2 \sim \mathcal{T}$  be the composite of those transformations, and  $\hat{\mathbf{x}}_1$  and  $\hat{\mathbf{x}}_2$  be the transformed images:

$$(\hat{\mathbf{x}}_1^{RGB}, \hat{\mathbf{x}}_1^D) = \mathbf{T}_1(\mathbf{x}_1^{RGB}, \mathbf{x}_1^D), \quad (2)$$

$$(\hat{\mathbf{x}}_2^{RGB}, \hat{\mathbf{x}}_2^D) = \mathbf{T}_2(\mathbf{x}_2^{RGB}, \mathbf{x}_2^D). \quad (3)$$

The output is a pair of multimodal images  $((\hat{\mathbf{x}}_1^{RGB}, \hat{\mathbf{x}}_1^D), (\hat{\mathbf{x}}_2^{RGB}, \hat{\mathbf{x}}_2^D))$  representing two augmented views of people under different natural variations.

##### 3) Multimodal Feature Extraction & Fusion

The *MFEF* module extracts and fuses features from the aforementioned pairs of RGB-D transformed views to produce RGB, depth, and RGB-D person representations. It consists of two networks [26]: 1) encoder  $\mathbf{f}_q$ , and 2) momentum encoder  $\mathbf{f}_k$ . Each RGB-D image pair is passed into both networks to extract these three representations:

$$\mathbf{q}_i^{RGBD}, \mathbf{q}_i^{RGB}, \mathbf{q}_i^D = \mathbf{f}_q(\hat{\mathbf{x}}_i^{RGB}, \hat{\mathbf{x}}_i^D; \theta_q), \quad i \in \{1, 2\} \quad (4)$$

$$\mathbf{k}_i^{RGBD}, \mathbf{k}_i^{RGB}, \mathbf{k}_i^D = \mathbf{f}_k(\hat{\mathbf{x}}_i^{RGB}, \hat{\mathbf{x}}_i^D; \theta_k), \quad i \in \{1, 2\} \quad (5)$$

where  $\theta_q$  and  $\theta_k$  are the weights of the network, and  $\mathbf{q}_i^{RGBD}, \mathbf{q}_i^{RGB}, \mathbf{q}_i^D$  and  $\mathbf{k}_i^{RGBD}, \mathbf{k}_i^{RGB}, \mathbf{k}_i^D$  are the feature representations of view  $i$  of each modality for the encoder, and momentum encoder, respectively. The encoder weights  $\theta_q$  are updated by back-propagation. The momentum weights  $\theta_k$  are updated by a weighted average of the weights  $\theta_q$  and  $\theta_k$  [26], where  $m$  is the momentum coefficient:

$$\theta_k \leftarrow m \theta_k + (1 - m) \theta_q. \quad (6)$$

Each encoder consists of separate RGB and depth backbones, fusion backbones, and multilayer perceptrons (MLPs), with weights  $\theta_l^{RGB}, \theta_l^D, \theta_l^{RGBD}, \theta_l^{MLP} \in \theta_l, l \in \{q, k\}$ , respectively. Each backbone uses a modified ResNet-18 model. The standard RGB ResNet-18 consists of 5 convolution blocks (C1-C5), fully connected (FC), and a SoftMax layer [39]. Our RGB and depth backbones extract RGB and depth specific features each using the first 3 convolution blocks (C1-C3), Fig. 1. A fusion backbone (purple layers) is incorporated to concatenate the feature maps of each of the C3 blocks, followed by a 1x1 convolution layer, and C4-C5, Fig. 1. MLPs, consisting of two FC layers, are added to the output of the fusion backbone to extract RGB-D representations. Additional MLPs are added to the output of

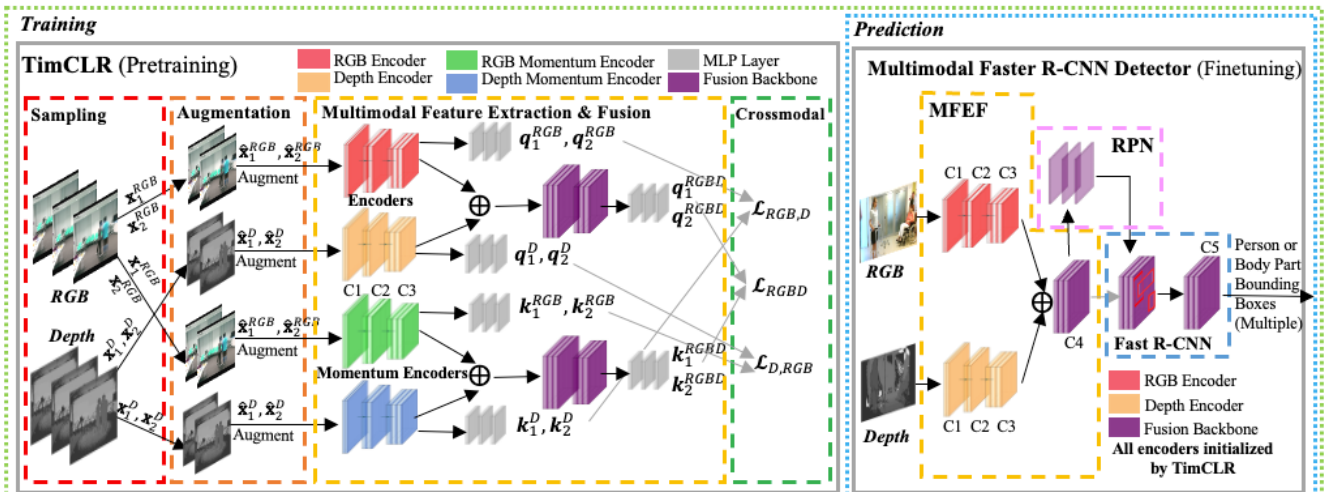


Fig. 1: Proposed multimodal DL detection architecture with first stage *TimCLR* and second stage *MFRCNN* detector.

the RGB and depth backbone layers to extract unimodal representations, Fig. 1. The output representations from the encoders  $(\mathbf{q}_i^{RGBD}, \mathbf{q}_i^{RGB}, \mathbf{q}_i^D)$ , and  $(\mathbf{k}_i^{RGBD}, \mathbf{k}_i^{RGB}, \mathbf{k}_i^D)$ ,  $i \in \{1, 2\}$  are passed to the *Crossmodal* module.

#### 4) Crossmodal

The *Crossmodal* module computes similarity scores of representations from both encoders. To measure similarity, the contrastive loss,  $\mathcal{L}_{CL}$ , based on InfoNCE is used [26]:

$$\mathcal{L}_{CL}(\mathbf{q}, \mathbf{k}) = \mathbb{E}_Q \left[ \log \frac{\exp(\mathbf{q}_i \cdot \mathbf{k}^+ / \tau)}{\exp(\mathbf{q}_i \cdot \mathbf{k}_i^+ / \tau) + \sum_{k^-} \exp(\mathbf{q}_i \cdot \mathbf{k}_i^- / \tau)} \right], \quad (7)$$

where  $Q = \{\mathbf{q}_1, \dots, \mathbf{q}_N\}$  is the set of representations from the mini-batch;  $\{\mathbf{k}_1^+, \dots, \mathbf{k}_N^+\}$  and  $\{\mathbf{k}_1^-, \dots, \mathbf{k}_N^-\}$  are the set of representations corresponding to the positive and negative image pairs, respectively; and  $\tau$  is the temperature [26]. The multimodal contrastive loss to measure similarity between RGB-D representations is:

$$\mathcal{L}_{RGBD} = \mathcal{L}_{CL}(\mathbf{q}_1^{RGBD}, \mathbf{k}_2^{RGBD}) + \mathcal{L}_{CL}(\mathbf{q}_2^{RGBD}, \mathbf{k}_1^{RGBD}). \quad (8)$$

The crossmodal contrastive losses to measure similarity between unimodal RGB and depth representations are:

$$\mathcal{L}_{RGB,D} = \mathcal{L}_{CL}(\mathbf{q}_1^{RGB}, \mathbf{k}_2^D) + \mathcal{L}_{CL}(\mathbf{q}_2^{RGB}, \mathbf{k}_1^D), \quad (9)$$

$$\mathcal{L}_{D,RGB} = \mathcal{L}_{CL}(\mathbf{q}_1^D, \mathbf{k}_2^{RGB}) + \mathcal{L}_{CL}(\mathbf{q}_2^D, \mathbf{k}_1^{RGB}). \quad (10)$$

The full contrastive loss which is the combination of all the aforementioned losses is defined as:

$$\mathcal{L}_{MCL} = \lambda_{RGBD} \mathcal{L}_{RGBD} + \lambda_{RGB,D} \mathcal{L}_{RGB,D} + \lambda_{D,RGB} \mathcal{L}_{D,RGB}, \quad (11)$$

where  $\lambda_{RGBD}$ ,  $\lambda_{RGB,D}$ , and  $\lambda_{D,RGB}$  are the weighting factors. The encoder weights  $\theta_q$  are passed to the *MFCNN* stage.

#### B. Multimodal Faster R-CNN

*MFCNN*, Fig. 1, adopts its structure from *FRCNN*. It consists of a *MFEF*, *RPN*, and *Fast R-CNN* module. Given an RGB and depth image, *MFEF* extracts feature maps using separate RGB and depth backbones each consisting of C1-C3 blocks which are initialized by  $\theta_q^{RGB}$  and  $\theta_q^D$ , the encoder weights of the unimodal backbones in *TimCLR*. These backbones are fused by channel-wise concatenation with a 1x1 convolution layer, followed by a C4 block. C4 is the input to both the *RPN* module, which generates person or body part bounding box proposals, and the *Fast R-CNN* module which uses C5 and these proposals for person classification and refinement. Both the C4 and C5 blocks are initialized by  $\theta_q^{RGBD}$ , the encoder weights of the fusion backbone in *TimCLR*. The *MFCNN* is first trained through supervised learning and used during prediction to output a bounding box for each detected person or body parts within an image.

## IV. EXPERIMENTS

The performance of our proposed two-stage person detection architecture is investigated in two sets of experiments: 1) a detailed comparison study with respect to existing robot person detection methods to evaluate detection accuracy, and 2) an ablation study to validate the design choices of our architecture. Two environments with varying levels of person occlusion, illumination, and deformation are considered. One environment is crowded with people and the other is cluttered

with objects, for which RGB-D images have been taken by a mobile robot. All experiments were conducted on a workstation with two RTX 3070 GPUs, an AMD Ryzen Threadripper 3960X, and 128GB of memory.

#### A. RGB-D Datasets

For the pretraining stage *TIMCLR*, the unlabelled **NTU RGB+D 120 Action Recognition (NTU) Dataset** [40] is used. The dataset consists of multiple people performing 120 different types of actions (e.g., standing, eating, jumping) in indoor environments with 114,480 RGB-D video samples collected by a Kinect sensor. This dataset naturally captures the intraclass variations that would be expected in a real-world human-centered environment.

We finetune the *MFCNN* detector through supervised learning and evaluate the detector on the **Mobility Aids (MA) dataset** [8] which consists of 17,000 annotated RGB-D images of multiple dynamic people undergoing frequent occlusions in a crowded real-world hospital environment. The dataset was collected by a mobile robot with a Kinect sensor. The original dataset contains 5 classes for people with different aids, which we combined into 1 person class to detect people. The dataset was split into 65/35 for training/testing, with separate sequences used in each set. The two test sets (TS): 1) TS1 (few people occlusions), and 2) TS2 (frequent people occlusions).

Our own **Urban Search and Rescue Person (USAR) dataset** [9] consisting of 570 RGB-D images of both human and mannequin body parts in a real-world cluttered environment was also used to finetune and evaluate the *MFCNN* detector. The images were obtained from a Kinect sensor onboard a Turtlebot 2 robot. The images contain 6 classes: arm, foot, hand, head, leg, and torso. The dataset was split using an 80/20 rule, with 3 separate test datasets collected on different days: 1) TS1 (contains fully visible people), TS2 (contains partial person or body part occlusions and deformations), and 3) TS3 (contains people under low lighting conditions).

#### B. Performance Metrics

The mean average precision (mAP) was chosen as the performance metric. The Intersection over Union (IoU) measures the area overlap between the ground truth and predicted bounding box.  $AP_{50}$  is the mAP where predictions with an IoU > 0.5 are considered true positives.  $AP_{0.5:0.95}$ , or AP, is the averaged mAP over IoU = {0.5, 0.55, ..., 0.95}. Averaging across IoUs more accurately measures localization [34], and will be considered the primary accuracy metric.

#### C. Training

The proposed person detection architecture is trained in two stages: 1) pretraining (*TimCLR*), and 2) finetuning (*MFCNN*). *TimCLR* was pretrained on a subset of the NTU dataset, consisting of a total of 1 million RGB and depth images. To generate this subset, videos were randomly selected from the 114,480 videos in the dataset. During training, image pairs were sampled at  $\Delta_t = 50$  frames. *TimCLR* uses the default hyperparameters from MoCo v3, and was trained for 100 epochs. *MFCNN* was finetuned using the pretrained weights from *TimCLR* on the MA dataset which



represents a crowded environment. All layers were finetuned using stochastic gradient descent (SGD) with a learning rate of 0.0025 for 130,000 iterations. Additionally, we finetuned *MFRCNN* on the USAR dataset to incorporate a cluttered environment using the same learning rate for 20,000 iterations.

#### D. Comparison Methods

Our person detection method was compared against existing DL RGB person detection methods: 1) RGB YOLO v2 [30], 2) RGB YOLO v3 [20], 3) RGB SSD [21], 4) RGB RetinaNet [9], and 5) RGB FRCNN [7]–[9]; 6) the depth-only ColorJet (CJ) FRCNN method [7], [8] which uses ColorJet to preprocess the depth images into 3-channels; and 7) the RGB-D Compression (Comp.) FRCNN method [9] which uses compression to preprocess RGB-D images. We have also designed 8) a strong baseline RGB-D CJ-MFRCNN which extends the depth-only CJ-FRCNN to include our *MFRCNN* network. Namely, the RGB and depth backbones use pretrained ImageNet weights, with ColorJet preprocessing on the depth images. All the networks were pretrained using a ResNet-18 backbone on ImageNet for 100 epochs.

#### E. People Detection Comparison Results

The detection accuracy results for our proposed method and all comparison methods on the test sets are presented in Table I. Our proposed *TimCLR+MFRCNN* detector outperformed all the other methods with respect to AP and AP<sub>50</sub> on all test sets (TS), including with intraclass variations of 1) partial occlusions (MA/USAR TS2), 2) deformations (USAR TS2), and 3) varying illuminations (USAR TS3). The results show *TimCLR*'s ability to learn invariant person features during pretraining. Worth noting is that our method outperformed the RGB-D CJ-MFRCNN which uses the same second stage detector, but off-the-shelf pretrained weights. Our *TimCLR+MFRCNN* was more robust to partial occlusions with a 5% improvement on AP (47.03 compared to 44.66), and a 4% improvement with AP<sub>50</sub> (75.23 compared to 72.52). These results are statistically significant, Table II. Our method also outperformed the unimodal networks such as YOLO, RetinaNet, and SSD with an AP of 47.03 compared to 35.82, 42.42, and 26.18, respectively, under partial occlusions. While the RGB-only approaches generally outperformed the depth-only CJ-FRCNN method, they performed worse under varying illuminations (USAR TS3).

In comparison to the RGB-D Comp. FRCNN, our method had greater improvement of up to 21% on AP, compared to only a 2% improvement on the AP<sub>50</sub>. This suggests that RGB-

D Comp. FRCNN predicts many correct bounding boxes of people with a 50% overlap with the ground truth, but it performs poorer when considering overlaps of larger than 50%, which the AP metric captures. One possible reason is that it had difficulties in estimating the extent of a person/body part under partial occlusions, as visual features may be lost during compression. Thus, our proposed method can accurately localize multiple people and body parts with a greater overlap between the predictions and ground truth.

Fig. 2 presents example detections of our *TimCLR+MFRCNN* method (Fig. 2(a)) compared to the two multimodal methods of RGB-D CJ-MFRCNN (Fig. 2(b)) and RGB-D Comp. FRCNN (Fig. 2(c)). The figure shows how these methods perform under partial occlusions (rows 1-3), pose deformation (rows 2-3), and poor lighting (row 3), on the MA (row 1) and USAR (rows 2-3) datasets. Our method identified all three people in Fig. 2 (a), especially the person on the right (which was missed by both the other detectors); and it was the only method to detect the partially occluded right foot in the second and third scenes. While RGB-D CJ-MFRCNN detected a part of the leg in Fig. 2(b), it did not capture the articulated portion of the leg as our method did. Under low lighting, only our method detected both feet and the articulated arm in the third scene.

A non-parametric Kruskal-Wallis test was performed on both the MA and USAR datasets, showing a statistically significant difference in AP between the multimodal methods and best performing RGB (FRCNN) and depth method (CJ-FRCNN), Table II. A post-hoc Dunn test with Bonferroni correction applied showed our method had a statistically significant AP than these alternatives, Table II.

#### F. Ablation Study

We performed an ablation study to evaluate the design of our proposed detection architecture. Namely, we investigated *TimCLR* with respect to the following: 1) image pair generation, 2) fusion design, and 3) effects of crossmodal loss. We evaluated each design choice based on the detection accuracy obtained by *MFRCNN* using the pretrained weights from *TimCLR*. We present these results in Table III.

In experiment 1, we investigated the following ways to generate positive image pairs, using: 1) only synthetic data augmentation, 2) only natural variations, and 3) a combination of both. We noticed that pretraining with only data augmentation outperforms training with only natural variations on TS1 as a result of feature suppression. However, they perform similarly under intraclass variations (TS2-3). During feature suppression, the network may ignore texture

TABLE I COMPARISON OF DETECTION ACCURACY OF OUR PROPOSED DETECTION METHOD VERSUS EXISTING DETECTION METHODS

Method \ Dataset	Mobility Aids (MA)				USAR					
	Test Set 1		Test Set 2 Occlusion		Test Set 1		Test Set 2 Occlusion+Deformation		Test Set 3 Illumination	
	AP	AP <sub>50</sub>	AP	AP <sub>50</sub>	AP	AP <sub>50</sub>	AP	AP <sub>50</sub>	AP	AP <sub>50</sub>
RGB-D TimCLR+ MFRCNN	58.68	93.94	47.03	75.23	21.90	45.68	17.84	40.17	18.40	36.90
RGB YOLO v2 [30]	34.17	84.34	24.89	67.20	7.76	28.82	7.56	30.91	8.00	30.11
RGB YOLO v3 [20]	38.82	92.03	35.82	74.30	16.85	33.11	14.50	33.75	15.30	31.31
RGB SSD [21]	35.19	86.95	26.18	70.96	10.43	29.68	9.83	32.15	8.44	30.41
RGB RetinaNet [9]	51.19	92.88	42.42	74.95	13.34	34.74	14.21	32.89	13.45	27.20
RGB FRCNN [7-9]	55.88	92.63	44.59	74.48	14.57	36.84	15.47	35.56	9.89	29.70
Depth ColorJet (CJ) FRCNN [7-8]	41.55	84.23	33.83	69.76	10.65	25.23	9.583	24.23	16.96	34.42
RGB-D Compression FRCNN [9]	48.36	93.58	39.18	74.10	15.27	38.27	15.12	37.78	17.77	34.40
RGB-D ColorJet (CJ) MFRCNN	57.85	92.58	44.66	72.52	20.39	43.78	16.60	38.37	17.70	35.23

TABLE II KRUSKAL-WALLIS AND DUNN TEST

Kruskal-Wallis Test				
<i>H</i> statistic for AP between these methods ( <b>TimCLR+MFRCNN</b> , <b>RGB-D CJ-MFRCNN</b> , <b>RGB-D Comp. FRCNN</b> , <b>RGB FRCNN</b> , <b>depth-only CJ-FRCNN</b> ), $p < 0.001$				
Mobility Aids		USAR		
Test 1	Test 2	Test 1	Test 2	Test 3
$n = 10795$	$n = 6238$	$n = 913$	$n = 905$	$n = 315$
21516	6231	529	498	260
Dunn Test with Bonferroni Correction				
<i>Z</i> statistic for AP between <b>ours</b> and the alternatives, $p < 0.001$				
Mobility Aids		USAR		
Test 1	Test 2	Test 1	Test 2	Test 3
2.98	12.05	3.09	3.38	3.09
21.27	25.35	3.49	4.42	6.54
30.87	28.89	11.15	9.69	9.64
84.01	36.15	17.23	15.84	15.34

or shape features as other cues such as color distributions which are similar between frames captured within a short interval can be used to differentiate positive pairs from negative pairs. The combined approach avoids this issue as it applies color jittering, while still being able to incorporate natural variations. Thus, it achieves higher detection accuracy under intraclass variations. In experiment 2, we investigated the fusion of RGB and depth features at C3, C4, or C5 blocks of the encoder. We found that fusing at progressively deeper layers leads to poorer accuracy in general, with C3 being the optimal layer to fuse. Finally, we investigated the effects of crossmodal contrastive loss which contrasts representations

between RGB and depth, for the purpose of evaluating the transfer of knowledge between modalities. We performed runs with and without this loss. The run with the crossmodal loss performed similarly on TS1, but substantially better under intraclass variations (TS2-3). One possible reason is that contrasting of features between modalities encourages representations between them to be similar, thus transferring learned feature invariances from one modality to the other.

## V. CONCLUSION

In this paper, we present a novel multimodal person detection architecture for mobile robots to address the robotic problem of person detection under intraclass variations. We introduce a new pretraining method *TimCLR* which learns person features which are invariant to natural variations in the environment, such as person and body part occlusions, pose deformations, and varying lighting conditions. Our *TimCLR* generates contrastive image pairs by sampling natural variations from multimodal image sequences within a short temporal interval, in addition to data augmentation. These invariant person features are used by a subsequent *MFRCNN* stage for robust detection of people under intraclass variations. Extensive experiments verified that our *TimCLR*+*MFRCNN* outperformed the existing detection methods in finding people in both crowded hospital and cluttered USAR environments. Our ablation study validated our use of a multimodal feature fusion approach. Our future work includes integrating our detection architecture within a mobile robot



Fig. 2: Multimodal detection results from: (a) TimCLR+MFRCNN (**ours**), (b) RGB-D CJ-MFRCNN, (c) RGB-D Comp. FRCNN; overlaid on RGB images.



TABLE III ABLATION STUDY

Method	Dataset	Mobility Aids (MA)				USAR				
		Test Set 1		Test Set 2 Occlusion		Test Set 1		Test Set 2 Occlusion+Deformation		Test Set 3 Illumination
		AP	AP <sub>50</sub>	AP	AP <sub>50</sub>	AP	AP <sub>50</sub>	AP	AP <sub>50</sub>	AP
TimCLR, data augmentation only		57.45	92.60	43.76	69.81	20.22	44.62	14.40	36.64	16.67
TimCLR, natural variations only		48.36	93.59	39.18	68.41	18.67	42.15	14.94	35.07	15.02
TimCLR, combined		58.68	93.94	47.03	75.23	21.90	45.68	17.84	40.17	18.40
TimCLR, C3 Fusion		58.68	93.94	47.03	75.23	21.90	45.68	17.84	40.17	18.40
TimCLR, C4 Fusion		57.65	92.44	44.29	68.63	21.01	44.23	17.40	39.64	17.78
TimCLR, C5 Fusion		53.69	89.73	42.94	68.14	18.67	41.35	15.43	35.62	16.21
TimCLR, no crossmodal loss		57.38	92.31	46.01	74.63	18.70	42.14	14.90	34.93	15.03
TimCLR, with crossmodal loss		58.68	93.94	47.03	75.23	21.90	45.68	17.84	40.17	18.40

for real-time person search and detection in varying human-centered environments.

## REFERENCES

- [1] S. C. Mohamed, S. Rajaratnam, S. T. Hong, and G. Nejat, "Person Finding: An Autonomous Robot Search Method for Finding Multiple Dynamic Users in Human-Centered Environments," *IEEE Trans. Autom. Sci. Eng.*, vol. 17, no. 1, pp. 433–449, Jan. 2020.
- [2] S. F. R. Alves, M. Shao, and G. Nejat, "A Socially Assistive Robot to Facilitate and Assess Exercise Goals," *IEEE Int. Conf. on Robot. and Automation Workshop on Mobile Robot Assistants for the Elderly (MoRobAE)*, pp. 1–5, 2019.
- [3] C. Thompson, S. Mohamed, W.-Y. G. Louie, J. C. He, J. Li, and G. Nejat, "The robot Tangy facilitating Trivia games: A team-based user-study with long-term care residents," in *IEEE Int. Symp. on Robot. and Intell. Sensors (IRIS)*, 2017, pp. 173–178.
- [4] D. Dworakowski, C. Thompson, M. Pham-Hung, and G. Nejat, "A Robot Architecture Using ContextSLAM to Find Products in Unknown Crowded Retail Environments," *Robot.*, vol. 10, no. 4, 2021.
- [5] T. Wengelfeld, S. Muller, B. Lewandowski, and H.-M. Gross, "A Multi Modal People Tracker for Real Time Human Robot Interaction," *IEEE Int. Conf. on Robot and Human Interactive Commun. (RO-MAN)*, New Delhi, Oct. 2019, pp. 1–8.
- [6] R. Triebel *et al.*, "SPENCER: A Socially Aware Service Robot for Passenger Guidance and Help in Busy Airports," vol. 113, 2016, pp. 607–622.
- [7] A. Vasquez, M. Kollmitz, A. Eitel, and W. Burgard, "Deep Detection of People and their Mobility Aids for a Hospital Robot," *ArXiv*, 2017.
- [8] M. Kollmitz, A. Eitel, A. Vasquez, and W. Burgard, "Deep 3D perception of people and their mobility aids," *Robot. Auton. Syst.*, vol. 114, pp. 29–40, Apr. 2019.
- [9] A. Fung, L. Y. Wang, K. Zhang, G. Nejat, and B. Benhabib, "Using Deep Learning to Find Victims in Unknown Cluttered Urban Search and Rescue Environments," *Curr. Robot. Rep.*, vol. 1, pp. 1–11, 2020.
- [10] W. Ouyang *et al.*, "DeepID-Net: Deformable deep convolutional neural networks for object detection," *IEEE Conf. on Comput. Vis. Pattern Recognit.*, Boston, 2015, pp. 2403–2412.
- [11] H. Murase and S. K. Nayar, "Illumination planning for object recognition using parametric eigenspaces," *IEEE Trans. Pattern Anal. Mach. Intell.*, vol. 16, no. 12, pp. 1219–1227, Dec. 1994.
- [12] C.-S. Fahn, C.-P. Lee, and Y.-S. Yeh, "A real-time pedestrian legs detection and tracking system used for autonomous mobile robots," *Int. Conf. on Appl. Syst. Innov.*, 2017, pp. 1122–1125.
- [13] D. Sanz, A. Ahmad, and P. Lima, "Onboard robust person detection and tracking for domestic service robots," *Second Iberian Robotics Conference*, Cham, Switzerland, 2015, pp. 547–559.
- [14] Z. Yuan, Y. Zhang, and R. Duan, "RGB-D People Detection and Tracking from Small-Footprint Ground Robots," in *Int. Conf. on Control and Robot. (ICCR)*, Hong Kong, Sep. 2018, pp. 25–29.
- [15] W. Huang, B. Zhou, K. Qian, F. Fang, and X. Ma, "Real-Time Multi-Modal People Detection and Tracking of Mobile Robots with A RGB-D Sensor," *Robot. Mechatron.*, p. 6, 2019.
- [16] C. Tomasi, "Histograms of Oriented Gradients," (2015).
- [17] C. Zheng *et al.*, "Deep Learning-Based Human Pose Estimation: A Survey," *ArXiv*, Jan. 2022.
- [18] Y. LeCun, Y. Bengio, and G. Hinton, "Deep learning," *Nature*, vol. 521, no. 7553, pp. 436–444, May 2015.
- [19] A. Krizhevsky, I. Sutskever, and G. E. Hinton, "ImageNet classification with deep convolutional neural networks," *Commun. ACM*, vol. 60, no. 6, pp. 84–90, May 2017.
- [20] K. Agrawal and R. Lal, "Person Following Mobile Robot Using Multiplexed Detection and Tracking," in *Advances in Mechanical Engineering*, Singapore, 2021, pp. 815–822.
- [21] R. Algabri and M.-T. Choi, "Target Recovery for Robust Deep Learning-Based Person Following in Mobile Robots: Online Trajectory Prediction," *Appl. Sci.*, vol. 11, no. 9, Art. no. 9, Jan. 2021.
- [22] S. Ren, K. He, R. Girshick, and J. Sun, "Faster R-CNN: Towards Real-Time Object Detection with Region Proposal Networks," *ArXiv*, 2015.
- [23] D. Du, L. Wang, H. Wang, K. Zhao, and G. Wu, "Translate-to-Recognize Networks for RGB-D Scene Recognition," *ArXiv*, 2019.
- [24] S. Zia, B. Yüksel, D. Yüret, and Y. Yemez, "RGB-D Object Recognition Using Deep Convolutional Neural Networks," in *IEEE Int. Conf. on Comput. Vis. Workshops*, 2017, pp. 887–894.
- [25] X. Wang, A. Shrivastava, and A. Gupta, "A-Fast-RCNN: Hard Positive Generation via Adversary for Object Detection," *ArXiv*, 2017.
- [26] X. Chen, S. Xie, and K. He, "An Empirical Study of Training Self-Supervised Vision Transformers," *ArXiv*, Aug. 2021.
- [27] P. Sermanet *et al.*, "Time-Contrastive Networks: Self-Supervised Learning from Video," *ArXiv*, Mar. 2018.
- [28] J.-T. Huang *et al.*, "Cross-Modal Contrastive Learning of Representations for Navigation using Lightweight, Low-Cost Millimeter Wave Radar for Adverse Environmental Conditions," *IEEE Robot. Autom. Lett.*, vol. 6, no. 2, pp. 3333–3340, Apr. 2021.
- [29] X. Wang, L. Zhang, D. Wang, and X. Hu, "Person detection, tracking and following using stereo camera," in *Ninth Int. Conf. on Graphic and Image Processing*, 2018, vol. 10615, pp. 83–91.
- [30] L. Pang, Z. Cao, J. Yu, P. Guan, X. Chen, and W. Zhang, "A Robust Visual Person-Following Approach for Mobile Robots in Disturbing Environments," *IEEE Syst. J.*, vol. 14, no. 2, pp. 2965–2968, 2020.
- [31] J. Zbontar, L. Jing, I. Misra, Y. LeCun, and S. Deny, "Barlow Twins: Self-Supervised Learning via Redundancy Reduction," *ArXiv*, 2021.
- [32] S. Pirk, M. Khansari, Y. Bai, C. Lynch, and P. Sermanet, "Online Object Representations with Contrastive Learning," *ArXiv*, 2019.
- [33] T. Chen, S. Kornblith, M. Norouzi, and G. Hinton, "A Simple Framework for Contrastive Learning of Visual Representations," *ArXiv*, 2020.
- [34] T. Lin *et al.*, "Microsoft COCO: Common Objects in Context" *arXiv*, Feb. 2015.
- [35] S. Kruthiventi, P. Sahay, and R. Biswal, "Low-light pedestrian detection from RGB images using multi-modal knowledge distillation," *IEEE Int. Conf. Image Process.*, 2017, pp. 4207–4211.
- [36] L. Spinello and K. Arras, "People Detection in RGB-D Data," *IEEE Int. Conf. Intell. Robots Sys.*, pp. 3838–3843, 2011.
- [37] L. Brigato and L. Iocchi, "A Close Look at Deep Learning with Small Data," *ArXiv*, 2020.
- [38] T. Chen, C. Luo, and L. Li, "Intriguing Properties of Contrastive Losses," *ArXiv*, 2021.
- [39] K. He, X. Zhang, S. Ren, and J. Sun, "Deep Residual Learning for Image Recognition," *ArXiv*, Dec. 2015.
- [40] A. Shahroudy, J. Liu, T. Ng, and G. Wang, "NTU RGB+D: A Large Scale Dataset for 3D Human Activity Analysis," in *IEEE Conf. Comput. Vis. Pattern Recognit.*, 2016, pp. 1010–1019.